Numerical study of the spark ignition of hydrogen-air mixtures at ambient and cryogenic temperature

Donatella Cirrone, Dmitriy Makarov, Christophe Proust, Vladimir Molkov

International Journal of Hydrogen Energy 79 (2024) 353–363

Contents lists available at ScienceDirect

International Journal of Hydrogen Energy

journal homepage: www.elsevier.com/locate/he

Numerical study of the spark ignition of hydrogen-air mixtures at ambient and cryogenic temperature

Donatella Cirrone [a,*], Dmitriy Makarov [a], Christophe Proust [b,c], Vladimir Molkov [a]

[a] HySAFER Centre, Ulster University, Newtownabbey, Northern Ireland, BT37 0QB, UK
[b] Institut National de l'Environnement Industriel et des Risques, Parc Technologique ALATA, BP2, 60550, Verneuil-en-Halatte, France
[c] Sorbonne University, Laboratory TIMR, UTC/ESCOM, Centre Pierre Guillaumat, 60200, Compiegne, France

ARTICLE INFO

Handling Editor: Dr J Ortiz

Keywords:
Computational fluid dynamics
Numerical model
Validation
Ignition energy
Spark ignition
Hydrogen safety
Cryogenic temperature

ABSTRACT

An accurate determination of minimum ignition energy (MIE) is essential for assessing electrostatic hazards and characterising potential for occurrence of combustion in flammable mixtures. This is of utmost importance for hydrogen-air mixtures characterised by a MIE equal to 0.017 mJ, whereas conventional flammable gases are characterised by MIE typically higher than 0.1 mJ. The study aims at developing and validating a CFD three-dimensional model capable to simulate complex unsteady physical and chemical phenomena underlying capacitive discharge spark. The model accounts for the experimental apparatus details, including the effect of electrodes' gap and associated heat losses. The numerical approach accurately reproduced the experimental measurements of MIE for mixtures of hydrogen with air at initial temperature ranging from ambient (T = 288 K) to cryogenic (T = 123 K). Hydrogen concentration in air was included in the range 10–55% for tests at T = 288 K, and 20–60% for tests at T = 173 K and 123 K respectively. Simulations assess the impact of experimental characteristics and design, such as the electrodes' dimension, and numerical features on process dynamics, growth of the flame kernel and MIE predictions.

1. Introduction

The evaluation of minimum ignition energy (MIE) is fundamental for assessing electrostatic hazards and characterising the occurrence of combustion in flammable mixtures. The MIE of combustible substances is defined as the minimum electrical energy stored in a capacitor leading to ignition of a quiescent mixture in the most ignitable composition [1]. The most common technique to measure MIE is the capacitive spark discharge, since the latter is also the most recurring electrostatic ignition source in practical applications [2,3]. A spark from a discharge circuit through inductive coils, used in industrial apparatuses and engines, is generally considered as a sequence of two stages: first a very rapid discharge with a high voltage potential called "capacity component", and then discharge under an almost constant and low potential applied for a longer period called "inductance component" [4]. Experimental studies attempting to assess which component contributes more to the ignition occurrence concluded that they can contribute similarly provided that a component has enough energy to ignite [4]. Early experiments on determination of the ignition energy (IE) for flammable mixtures were performed in Refs. [5,6]. Conventional flammable gases, e.g. methane, have MIE values typically larger than 0.1 mJ. Conversely, experiments for hydrogen-air mixtures recorded MIE as low as 0.017 mJ [7,8]. The MIE measurements may also be significantly affected by the experimental set-up and design, as noted by Kutcha [9] in comparison with data in Refs. [5,6] for lean mixtures. It should be noted that in the experiments not all the nominal energy stored in the circuit is applied for igniting the gas mixture, but a portion of it is lost, e.g., in the circuit resistance. Losses were observed to depend on the circuit resistance and discharge time, reporting that up to 95% of the energy could be delivered into the gas [10]. Experiments in Ref. [8] reported that more than 99% of the stored energy was released in the discharges. Nevertheless, experiments in Ref. [11] for a 5 pF capacitance reported a high variability of actual energy released into the spark gap: it varied from 50% to 90% of the stored energy when passing from a 50 kΩ to a 100 Ω resistor respectively. The distance between the electrodes' tips, hereby named as gap size or distance (L_{gap}), affects the measured MIE. In 2007, Ono et al. performed an extensive experimental campaign to assess the IE curve for mixtures of hydrogen with air by varying the composition and L_{gap} in the range 0.5–4.0 mm [8]. The global MIE of 0.017 mJ was found for L_{gap} = 0.5 mm and hydrogen concentration within 22–26% by vol. in air. For

* Corresponding author.
E-mail address: d.cirrone@ulster.ac.uk (D. Cirrone).

https://doi.org/10.1016/j.ijhydene.2024.06.362
Received 20 March 2024; Received in revised form 20 May 2024; Accepted 26 June 2024
Available online 6 July 2024

this range of concentration and low energies, the MIE increased for larger gap distances due to greater heat losses from the larger spark channel surface and lower energy density. On the other hand, an opposite trend was observed in experiments towards the flammability limits, where the shorter gap lengths provided higher MIE. This is believed to be due to a not sufficient quantity of flammable mixture excited by the released energy to sustain the flame development. An increase of oxygen concentration in the oxidiser leads to a decrease of measured MIE. Kumamoto et al. [2] recorded a MIE equal to 0.0057 mJ for a concentration of 35% by vol. of O_2 in air, whereas Kutcha [9] assessed a value of 0.0012 mJ for hydrogen-oxygen mixtures. Oxygen concentration in air can decrease significantly in the event of unintended cryogenic hydrogen leaks (including LH_2), as O_2 condensation may occur locally before nitrogen condensation. This could increase the MIE and can be taken as explanation why no spontaneous ignition occurred in all NASA tests on LH_2 releases [12]. On the other hand, experiments in Ref. [13] observed occurrence of a highly-energetic secondary explosion upon ignition of a LH_2 jet, which was deemed to be caused by reaction of hydrogen with accumulated condensed oxygen (LO_2).

The spark ignition is an unsteady process characterised by a complex underlying physics and chemistry, which involves ionisation of the spark gap and plasma formation with temperatures as high as 60,000 K [14]. Several ignition systems and circuits can be used to realise the spark ignition. Nevertheless, the sequence of processes initiated by the spark ignition can be outlined as follows, based on the work [14]:

- The "*breakdown phase*" is characterised by the highest spark currents and voltages. This phase lasts few nanoseconds. The applied voltage causes the ionisation and electronic excitation of the gas in the spark gap, leading to a very rapid heating of the gas with temperature up to 60,000 K [14]. After the spark breakdown, a very thin plasma channel (10–100 μm in radius) forms between the electrodes tips [15].
- The "*arc phase*" is characterised by a drop of voltage by even two orders of magnitude. This phase is determined by the capacitive and inductive components of the spark. This phase is steadier and lasts about 1 μs. The core temperature of the formed spark channel decreases to about 5000–6000 K [14].
- The "*glow phase*" involves the release of the remaining stored electrical energy under a current mainly controlled by the coil impedance with approximately linear decrease in time. This phase lasts about 1–2 ms. The spark channel core temperature decreases to about 3000 K [14].

The three phases listed above constitute the basic discharge modes of a spark ignition process and they can be present in different combinations and provide varying contributions depending on the specific electrical circuit layout. Chemical reactions are already triggered during the breakdown phase. The far too high temperature of the channel core can hinder a stable generation of combustion products, whereas the plasma surface is more likely to present the conditions to initiate the combustion reactions by spreading heat and radicals to the flammable mixture. If the combustion reactions become self-sustained once the spark energy discharge is ceased, the ignition is deemed to be successful. It should be highlighted that a spark discharge is a particularly short and intense process in particular for low energy discharges. Kumamoto et al. [2] indicated that the spark duration in experiments on ignition of hydrogen-air mixtures was lower than 100 ns. Ono et al. [8] reported spark durations lower than 20 ns for energy discharges below 0.035 mJ, whereas duration could increase to the order of milliseconds for increasing resistance of the electrical circuit. Liberman [16] indicated a range as wide as 0.01–100 μs for spark energy discharge processes.

Computational Fluid Dynamics (CFD) is a valuable tool capable of providing insights into the phenomenon of spark ignition of flammable mixtures and the flame kernel development. Nevertheless, numerical simulation of this phenomenon is particularly challenging because of the underlying complex and unsteady physics and chemical kinetics, occurrence of extremely high temperatures and gradients, rapid processes, etc. Frendi and Sibulkin in 1990 [17] carried out one the first studies on modelling spark ignition for methane-air mixtures. The numerical study neglected radiation and conductive losses, assumed deposition of discharged energy in a spherical kernel and a 1-step chemical reaction. Numerical prediction of MIE for a spark with radius of 63 μm and duration of 27.5 μs underpredicted experimental measurements by a factor of 70, though simulation for a radius of 500 μm resulted in a closer agreement with experiments. In 2002, Thiele et al. [18] conducted an experimental and two-dimensional (2D) numerical investigation on spark ignition with more detailed characterisation of the reacting flow for hydrogen-air mixtures considering 38 reactions. The numerical approach included coupling of equations of the flow and spark electrodynamics, well reproducing the transition to an established propagating flame. Simulation results for an energy discharge lasting 50 μs showed that expansion of the hot core dominates the process up to 80 μs, at which point the flame starts detaching from the spark kernel with speed characteristic for flame propagation. The authors [18] observed that losses to the electrodes did not affect the simulation results up to 130 μs. In 2002, Yuasa et al. [19] used 2D numerical simulations to estimate the impact of the energy release in terms of ratio of capacitive spark energy component over the total MIE for methane-air mixtures. Durations of the capacitive spark discharge and inductance spark were assumed to be 1 μs and 100 μs respectively. Further numerical investigations on determination of MIE for methane-air mixtures were performed in 2009–2010 by Han et al. [20, 21] and it was concluded that the size of electrodes assumed in computations could greatly affect the resulting MIE. The same conclusion was confirmed for hydrogen-air mixtures in 2011 by Han et al. [22], where the authors performed 2D simulations to determine the MIE by employing 53 species and 325 elementary reactions. Simulation results assessed the effect of different factors on ignition dynamics. To obtain a successful ignition, the deposited energy shall be high enough to heat up the unburnt mixture portion around the spark channel to the temperature of the flame and ensure the activation of chemical reactions producing enough heat to exceed the energy losses to the electrodes and losses from the surface of the spark channel, as indicated in Ref. [6]. The latter can be affected by the dimensions of the spark core assumed for the calculations, as observed in the numerical work [22]. The authors in Ref. [22] assessed that, for a stoichiometric mixture of hydrogen with air and channel radius lower than 150 μm, the MIE stabilised to the value of 0.04 mJ, overestimating the experimental results by over 135%. A parametric assessment varying the gap distance between electrodes showed that the electrodes' sizing can considerably affect the prediction of MIE when L_{gap} is lower than the quenching distance for a given composition of the mixture (0.66 mm [22]), whereas effect was negligible for gap lengths larger than the quenching distance. Han et al. [22] numerically investigated the effect of the energy supply procedure and thus energy density on the ignition of flammable mixtures. The authors tested three models for the energy supply procedure where the spark channel was either kept constant to 0.3 mm or allowed to increase in two and four steps up to the value of 0.3 mm for a given ignition energy and duration. The authors observed that the energy supply procedure for methane-air mixtures did not affect the temperature history for the stage of the developed flame and the calculated MIE. On the other hand, the energy supply procedure considerably affected the results obtained for hydrogen-air mixtures, where the successful ignition was observed only for the four steps energy supply, characterised by highest energy density in the initial phase of the spark, and not for the other two energy supply models. It should be highlighted that a spark duration of 20 μs was used for the study. In 2023, Fernández-Tarrazo et al. [23] performed numerical simulations to determine MIE in hydrogen-air mixtures by assuming a spherical region for the energy deposition. The resulting MIE was seen to be approximately constant for a radius lower than 100 μm,

whereas beyond this limit MIE was seen to increase with growing radius. The authors concluded that gas compressibility effects need to be included to describe the formation of shock waves for short energy deposition time. Their simulations results were shown to underpredict MIE experimental measurements in Refs. [5,6,8,11]. The authors attributed this difference in predictions to the absence of electrodes in modelling, and thus the associated heat losses. It is inferred from previous studies in Refs. [22,23] that distancing the assumptions of the numerical studies from real experimental conditions may be the cause of inaccurate MIE estimations for mixtures of hydrogen with air up to now.

Current hydrogen storage and transport applications often employ liquid hydrogen (boiling temperature 20.3 K at ambient pressure) or cryo-compressed hydrogen ($T \leq 150$ K), due to the higher densities that can be achieved at lower temperatures [24]. In the event of loss of LH_2 containment or release of cryogenic hydrogen from the storage or equipment, there could be formation of hydrogen-air mixtures at temperature below atmospheric. While ignition hazards for hydrogen-air mixtures at ambient temperature have been extensively investigated, lesser studies have been performed on hazards for mixtures at cryogenic temperature. In 2023, Cirrone et al. [25] proposed a theoretical model to reproduce MIE experimental measurements for hydrogen-air mixtures with initial temperature in the range 123–290 K. Theoretical results confirmed the experimental observations of a slight increase of MIE for decreasing temperature of the mixture.

This research aims at developing a CFD three-dimensional (3D) approach to estimate numerically the MIE curve for varying concentration and temperature of the hydrogen-air mixture. The CFD approach includes modelling of radiation and heat losses to the electrodes. Simulations reproduce the experimental set-up in Ref. [8], including electrodes' dimensions and gap configuration. Experimental measurements in Refs. [6,8] are compared to simulation results to assess the predictive capability of the proposed numerical model for mixtures of hydrogen with air at ambient temperature. Furthermore, the CFD model validation was extended to mixtures at cryogenic temperature by comparison against the experimental tests performed by INERIS in the frame of PRESLHY project "Pre-normative Research for Safe Use of Liquid Hydrogen" funded by the Clean Hydrogen Partnership (Grant Agreement No. 779613) [25,26]. The contemporary CFD model is intended to complement the theoretical model published by the authors in 2023 [25]. While this theoretical model can predict accurately MIE for H_2-air mixtures requiring knowledge of only their composition and temperature, the CFD modelling is deemed to give insights into the spark ignition phenomenon, dynamics and flame kernel development. Simulations of a realistic experimental layout also allow to assess the effect on MIE of the testing design and characteristics, such as electrodes' dimension, conductive losses to the electrodes and radiative losses, etc.

2. Validation experiments

The experimental measurements used to build the MIE curve for mixtures of hydrogen with air at initial ambient temperature have been selected from the sets of experiments in Refs. [6,8,25]. Numerical simulations reproduce the experimental apparatus employed in Ref. [8], which used a capacitive spark discharge for mixtures with concentration in the range 7–68% of hydrogen by vol. in air. The needle to needle tungsten electrodes had diameter of 1.0 mm with a 40° angle tip ending with a diameter estimated to be in the range of 0.1–0.2 mm [27]. The MIE was measured for a variable gap distance between the electrodes. The MIE measurements for $L_{gap} = 0.5$, 1.0, 2.0 mm are used for comparison against numerical simulations for varying hydrogen concentration in air. Experiments in Ref. [6] were performed on mixtures with hydrogen concentrations in air within 7–57% vol. range. The gap between the needle-to-needle electrodes was 0.5 mm, whereas other characteristics are not known to the authors. In 2020, Proust [26] conducted experiments for mixtures with concentration range 10–50% vol. The tungsten electrodes had an ending diameter of 0.1 mm, whereas L_{gap} was equal to 0.5 mm. The same electrodes configuration was used for the tests performed at cryogenic temperature of 173 K for mixtures with composition 10%, 20%, 30% and 40% of hydrogen by vol. in air and at 123 K for the 40% composition reported in Ref. [25]. Further details on the experiments are available in Refs. [25,26,28].

3. CFD modelling approach

The CFD approach employs a pressure-based solver considering the flow as a laminar and compressible ideal gas following conclusions by Fernández-Tarrazo et al., in 2023 [23] to include gas compressibility effects to describe the formation of shock waves following the energy discharge in a short deposition time. The modelling of combustion employs the Finite Rate model with a detailed chemical kinetic mechanism [29] involving 13 species and 37 elementary reactions to describe in detail the ignition process and effect of multi-step reactions. The approach includes radiation modelling via the Discrete Ordinates (DO) model [30], as found to well represent radiation losses in Ref. [31] and hydrogen jet flames in Refs. [32,33]. ANSYS Fluent version 14.5 has been employed as a computational engine.

3.1. Assumptions and selection of simulation tests

The spark energy is discharged only as a capacitive component, given that it is the most recurrent method for MIE measurement [2]. Validity of this assumption is confirmed by Babrauskas in 2003 [10] stating that generally the capacitance and voltage of the circuit are used to measure the nominal energy. The spark is assumed to have a duration of 1 μs, as per the capacitive discharge in Ref. [19]. The chosen spark duration is also an intermediate value of the wider range of 0.01–100 μs indicated in Ref. [16]. The energy dissipation in the circuit is neglected and ionisation processes are not taken into account into modelling. The electrodes configuration in our simulations reproduce the experimental set-up in Ref. [8], considering tungsten electrodes with diameter equal to 1 mm. The electrodes' tip side is inclined by an angle of 40° with respect to the electrodes' symmetry axis, and it ends with a flat circular surface with diameter of 0.2 mm, whereas experiments could present a rounded tip. The energy discharge occurs in a cylindrical channel between the needle-to-needle electrodes. L_{gap} varies from 0.5 to 2.0 mm according to the experimental conditions in tests by Ono et al. [8] simulated in our study for $T_0 = 288$ K. Table 1 shows the electrode gaps used in the numerical tests for hydrogen concentration in air within the range of 10–55% vol. For the mixtures at cryogenic temperature, L_{gap} is 0.5 mm [26].

Table 2 reports the mixture composition for the simulations at cryogenic temperatures equal to 173 K and 123 K.

The spark discharge results in the formation of a very thin plasma channel with radius in the order of 10–100 μm [15]. The spark channel radius had been analytically estimated as 100 μm by Bane et al., in 2013 [34]. In 2018, Benmuffok et al. [35] gathered the data on initial radius of the spark channel indicated by different authors from the literature. The sources showed some differences with the spark channel radius varying from 100 μm to 200 μm. However, the majority of sources

Table 1
Hydrogen concentration in air and electrode gap distance in simulation tests at initial ambient temperature selected for comparison with experiments in Ref. [8], with exception for test 4 from Ref. [6].

Test	T_0, K	H_2 concentration, % vol.	L_{gap}, mm
1	288	10	2.0
2	288	14	1.0
3	288	22	0.5
4	288	29	0.5
5	288	35	1.0
6	288	45	1.0
7	288	55	2.0

Table 2
Hydrogen concentration in air and electrode gap distance in simulation tests at initial cryogenic temperature selected for comparison with experiments in Ref. [26].

Test	T_0, K	H_2 concentration, % vol.	L_{gap}, mm
1c	173	20	0.5
2c	173	30	0.5
3c	173	40	0.5
4c	173	60	0.5
5c	123	20	0.5
6c	123	30	0.5
7c	123	40	0.5
8c	123	60	0.5

indicated a spark channel radius of approximately 100 μm, similarly to Refs. [15,34]. Thus, a spark channel radius (R_c) equal to 100 μm is assumed in the present study for the determination of MIE. Nevertheless, preliminary simulations to assess the model sensitivity to numerical details and spark channel radius were conducted also for $R_c \leq 60$ μm and described in the section "Initial assessment of the model sensitivity to numerical and experimental details" below. Energy in the spark channel E is released uniformly in the cylindric volume V_{spark} by imposing a constant source term S_E to the energy equation, calculated as $S_E = \frac{E}{\Delta t \bullet V_{spark}}$ J/s/m^3, during the ignition time Δt. This assumption is in line with experimental observations of MIE resulting approximately constant for Δt = 5ns-1ms [8]. It is considered that modelling the spark discharge as an energy deposition in a cylindrical volume corresponding to the spark channel allows to assess the MIE, similarly to the theoretical approaches described in Ref. [25] where the MIE was estimated as the energy required to heat up the flammable mixture at initial temperature of the unburnt mixture to that of the flame and to compensate the heat losses from the surface of the mixture portion heated by the released energy.

3.2. Numerical details

Given the axisymmetric nature of the simulated flame kernel formation, only a latitudinal quarter of a sphere is considered as the calculation domain (see Fig. 1a). The hexahedral mesh has radius equal to 5 mm and is built through ICEM CFD 18.0 (see Fig. 1b) and control volumes (CV) had minimum orthogonal quality equal to 0.32. The minimum CV size in the numerical domain is 8 μm, which provided 12 CVs along the 100 μm radius of the spark cylindrical channel, shown in detail in Fig. 1c. The cell size is set to increase with a growth ratio of 1.05 towards the domain boundaries. The number of CVs in the numerical domain is approximately 138,600 for the simulation tests with L_{gap} equal to 0.5 mm, whereas it increases to approximately 184,000 for the tests with L_{gap} = 1.0 mm and 208,200 for L_{gap} = 2.0 mm. Sensitivity to the numerical grid refinement and symmetry angle will be demonstrated in section "Initial assessment of the model sensitivity to numerical and experimental details".

The solid electrodes are embedded in the numerical mesh to account for the associated conductive losses. Tungsten properties are applied for the electrodes, being the material used in the experiments: specific heat equal to 134 J/kg/K, density equal to 19,300 kg/m^3 and thermal conductivity equal to 173 W/m/K [36]. Conjugate heat transfer problem is solved on the electrode surfaces to ensure continued and smooth solution for temperature and heat fluxes on the fluid-solid boundary. The surface emissivity coefficient is assumed to be 0.032 as per tungsten aged filaments [37]. For each investigated case, the domain is initialised with composition and temperature given in Tables 1 and 2, and ambient pressure (101,325 Pa). A negligible velocity equal to 10^{-8} m/s is applied at initialisation, as suggested for compressible flows solution strategies in Ref. [38].

The external boundary (see Fig. 1a) is defined as a non-reflecting pressure outlet to avoid reflection of waves in the selected compressible solver and has same conditions as per the initialisation. A constant time step equal to 0.01 μs is used for the first 1 μs simulated time period to ensure 100 time steps throughout the discharge of the spark energy. Afterwards, the time step size is gradually increased and adapted in calculations to maintain a constant Courant Friedrichs Lewis (CFL) number through the original time step adapting technique presented in Ref. [39]. A CFL = 0.3 is employed in the numerical study.

The angular discretisation of the DO model employs 5x5 angular divisions, as shown to well represent effect of radiation losses in Ref. [31]. Water vapour is considered as the only emitting/absorbing gas substance in hydrogen-air combustion, as this assumption was seen to well represent emitted radiation by hydrogen jet fires in Refs. [32,33] with absorption coefficient determined following the data in Ref. [40]. The high temperature spark channel (T > 5000 K) is assumed to behave as a blackbody radiative source following the observations in Ref. [41]. Thus, an emissivity equal to 1 is considered for the mixture at temperature beyond 5000 K. To avoid sudden variation in the absorption and thus emissivity coefficient, a transition stage increases gradually the absorption coefficient up to 1 within the range of temperature

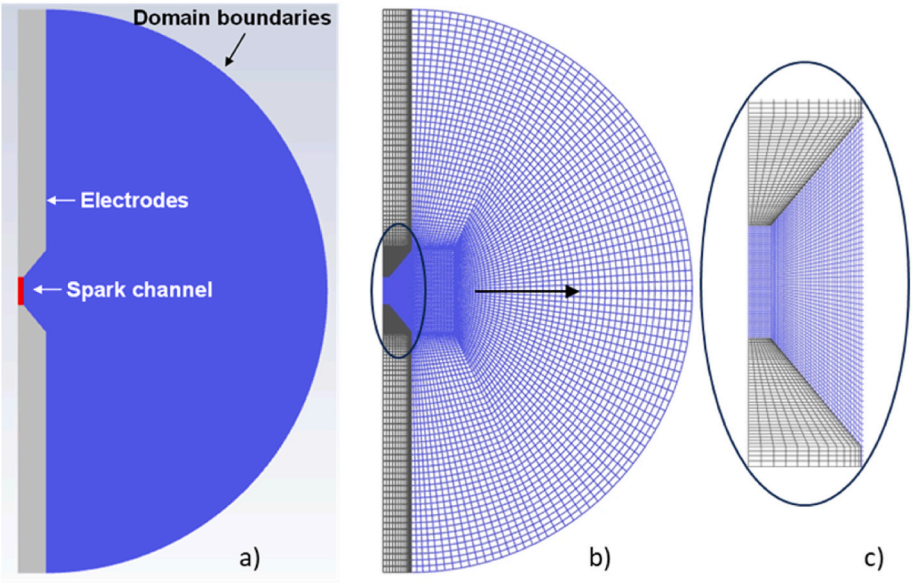

Fig. 1. Calculation domain on the x-y plane (a), numerical grid (b) and zoomed-in at the spark gap grid (c).

4000–5000 K.

The solver employs a PISO algorithm, as recommended for transient formulations and to reduce convergence difficulties associated with distorted meshes [38], and second-order upwind scheme for space discretisation.

4. Results and discussion

The scope of this study is to develop and validate a CFD approach for numerical prediction of MIE in mixtures of hydrogen with air capable to shed light on the spark kernel development process and flame propagation dynamics. Nevertheless, prior to proceeding with the core study, a comprehensive initial assessment has been performed to test the validity and suitability of the numerical details and physical assumptions described in Section "CFD modelling approach" and employed here for ignition and MIE modelling study. These characteristics will be highlighted and discussed in detail in Section "Initial assessment of the model sensitivity to numerical and experimental details".

4.1. Initial assessment of the model sensitivity to numerical and experimental details

The first assessment was performed on the sensitivity to the grid refinement and angle of symmetry for the numerical domain. Results for a grid with symmetry angle of 12° and minimum CV size equal to 4 μm (total 93,035 CVs for a 2 mm domain radial extension) are compared to outcomes of a grid with symmetry angle of 90° and minimum CV size equal to 8 μm. The numerical grids have been tested for the case of stoichiometric hydrogen-air mixture, $IE = 17$ μJ, $R_c = 60$ μm, $L_{gap} = 0.5$ mm and without presence of the electrodes in the domain. It is observed that the coarse mesh would result as expected in a "thicker" flame front, due to the numerical requirements of 3–5 CVs to represent discontinuities and gradients such as a flame front [39]. This effect is assessed to cause an approximately 6% longer distance reached by the flame front at 140 μs. Nevertheless, the difference in maximum temperature of the flame resulting from the two grids is negligible, and deviation in average flame front velocity is below 2%, verifying the achievement of the practical independence of solution on numerical grid. Thus, the coarser grid with symmetry angle of 90° is selected for the following simulations. Furthermore, grids with low symmetry angles of a sphere, despite decreasing the number of control volumes for finer grids, would be affected by high skewness and low quality of the numerical grid, which could be a reason for numerical oscillations and instabilities in such a challenging process.

A CFL number sensitivity assessment was conducted by analysing the effect of CFL decrease from 0.3 to 0.1 on the front of the propagating flame. The test with stoichiometric hydrogen concentration in air with $IE = 17$ μJ, $R_c = 60$ μm, $L_{gap} = 0.5$ mm in absence of the electrodes in the numerical grid to minimize losses was selected to perform a conservative assessment. The temperature distribution in time along the *x*-axis indicated that simulation for CFL = 0.3 results in a slightly slower flame front. The effect is seen to increase with time, yet at 156 μs, the average relative difference in the flame front velocity is about 4.5%, which is considered to be acceptable in comparison to the gain in computational time. Thus, a CFL = 0.3 was employed in the numerical study.

The high energy discharge may lead to the occurrence of temperatures higher than 10,000 K [4] in the spark channel, and thus significant radiation losses. A further simulation test was performed to compare two limiting cases in presence and absence of radiation modelling for a 55% hydrogen-air mixture, $IE = 45$ μJ, $R_c = 60$ μm, $L_{gap} = 2.0$ mm, $R_{el} = 0.1$ mm [8], where R_{el} is the radius of the electrodes. Simulations results showed that taking into account radiation can impact greatly the maximum temperature achieved during the energy release, causing a decrease from 7124 K to 5546 K, i.e., by almost 30%. The variation of temperature causes a corresponding decrease in produced maximum hydroxyl (OH) mole fraction by approximately 48%. Once this 55% hydrogen-air mixture is ignited, the flame temperature stabilises at about 1000 K, and the difference between the simulated temperature accounting for radiation losses or not decreases to approximately 9% at 100 μs. The effect of radiation losses increases significantly for larger releases of energy and narrower electrodes gaps, as observed for a simulation test with 10% hydrogen-air mixture, $IE = 110$ μJ, $R_c = 60$ μm, $L_{gap} = 0.5$ mm, $R_{el} = 0.1$ mm [6]. In this case the test without considering radiation losses reached a maximum temperature 4 times larger than the test including radiation into modelling (53,676 and 13,291 K respectively). The larger radiation losses are caused by the emissivity equal to 1 for the plasma above 5000 K and the higher temperature reached in the spark channel. As the energy discharge is ended and flame propagates outwards the spark channel, the maximum flame temperature stabilises at about 1500 K at 100 μs when radiation losses are considered, which is about 20% less than when radiation modelling is not included into simulation. Despite the effect on the dynamics of the maximum temperature reached throughout the simulation, the simulated MIE did not vary for the test with 10% hydrogen-air mixture and L_{gap} of 0.5 mm. The MIE for this test is determined by progressively decreasing the discharged energy by a factor of two. It should be remarked that an eventual more gradual decrease of discharged energy from one simulation to another may estimate more precisely MIE and possibly lead to a noticeable effect on MIE determination.

A similar approach was used to analyse the impact of conductive losses to the electrodes through comparison of two limiting domain configurations in presence and absence of electrodes. An electrodes' diameter of 1.0 mm was considered to maximise the effect of electrodes presence and conduct a conservative assessment. Simulation results showed a noticeable effect on MIE for lean H_2-air mixtures and $L_{gap} =$ 0.5 mm. A second analysis instead assessed the effect of the electrodes' tips diameter for the test with 10% hydrogen-air mixture with $IE = 30$ μJ, $R_c = 60$ μm, $L_{gap} = 2.0$ mm [8] by decreasing it from 1.0 mm to 0.2 mm. As expected, simulation results recorded lower temperature and OH concentration during the energy discharge for the larger electrodes diameter, due to greater heat losses to the electrodes. However, for both electrodes' sizes the mixture ignited for $IE = 30$ μJ, whereas it failed to ignite for $IE = 20$ μJ. The lack of variation in the MIE for $L_{gap} = 2.0$ mm is in line with conclusions of study [22], since L_{gap} is close to the quenching distance for this concentration [42] and thus may not be affected by the electrodes' size. Nevertheless, a more gradual decrease in IE may show potentially a different ignition limit also for $L_{gap} = 2$ mm.

The formation of a plasma channel during the breakdown phase is a very unstable and variable process. The assumption of suitable spark channel dimensions is essential for an accurate reproduction of the energy deposition and MIE estimation. A final assessment has been performed varying the spark channel radius for the case with 10% hydrogen-air mixture and $L_{gap} = 0.5$ mm by variation within the range indicated in Ref. [15] for the breakdown phase: $R_c = 20$ μm, $R_c = 40$ μm, $R_c = 60$ μm and $R_c = 100$ μm. A finer mesh with minimum CV size of 4 μm has been used for the cases with lower R_c to ensure at least 5 CVs along the spark channel radius. Simulation results showed that for $R_c \leq$ 60 μm the MIE levelled off to 9 μJ, whereas the mixture failed to ignite for energy $E = 6$ μJ. The case with $R_c = 100$ μm predicted a MIE equal to 15 μJ for the stoichiometric hydrogen-air mixture, whereas energy $E =$ 12 μJ failed to ignite the mixture. The simulated MIE is in perfect agreement with the widely accepted $MIE = 17$ μJ. A spark channel radius $R_c = 100$ μm is thus considered to be a better assumption to represent a spark channel size after the breakdown and during the arc phase in numerical simulations. This is also supported by majority of experimental observations presented in Ref. [35]. Therefore, spark channel radius $R_c = 100$ μm is selected and employed for the simulations of MIE in the following sections.

4.2. Validation of the CFD MIE model for hydrogen-air mixtures at ambient temperature

The numerical tests to estimate the MIE in a mixture of hydrogen with air at $T_0 = 288$ K are conducted according to the assumptions and numerical details described in Section "Assumptions and selection of simulation tests", namely $R_c = 100$ μm and $R_{el} = 0.1$ mm. The MIE is determined by a sequence of simulations for varying progressively the energy released in the spark channel. As an example, let us consider a stoichiometric hydrogen concentration in air with $R_c = 100$ μm and $L_{gap} = 0.5$ mm: after verifying ignition for IE = 17 μJ as observed in experiments [6], a simulation test was performed for IE reduced to 15 μJ, which still resulted in ignition. In a following simulation test, the IE was further reduced to 12 μJ resulting in failure to ignite the mixture and establishing 15 μJ as simulated MIE. The energy is discharged in the spark channel within 1 μs, causing a sharp rise of temperature to approximately 2300 K. Once the energy discharge is stopped, the mixture will undergo a rapid decrease of temperature due to the presence of losses, occurrence of thermal expansion and mixing with the unburnt components. The formation of a propagating flame is considered to verify the occurrence of ignition. The criteria used to indicate a successful ignition are the stable presence of hydroxyl (radical OH) mole fraction, high temperature and increase of water vapour integral mass. On the other hand, the ignition failure is considered to occur when the maximum temperature in the domain decreases below the limit value of 600 K, absence of stable radical OH generation and water vapour build up, similarly to our study [43]. Fig. 2 reports the example on MIE determination for the case with 29% hydrogen-air mixture. The maximum temperature rapidly increases to about 2300 K in the spark channel when an IE equal to 15 μJ is applied. As soon as the ignition source is stopped in 1 μs, the maximum temperature decreases to approximately 1300 K to then rise again once combustion becomes self-sustainable, as proved by the similar trend in maximum OH mole fraction and increasing water vapour integral mass. On the other hand, when an energy equal to 12 μJ is applied, the temperature reaches a maximum of approximately 1600 K, followed by a rapid decrease to the limit to ascertain ignition failure within 40 μs.

Simulations were performed for all the cases presented in Table 1 for ambient temperature mixtures. The values of energy leading to a successful or failed ignition are shown in Fig. 3. It can be observed that the mixture with hydrogen concentration in air within 22% and 29% vol. provides an absolute MIE equal to 15 μJ, whereas the mixture fails to ignite with deposited energy $E = 12$ μJ. The simulated absolute MIE well reproduces the experimental widely accepted MIE of 17 μJ. The experimental MIE curve for lean and rich compositions of the mixture is obtained for spark gaps larger than 0.5 mm. Simulations were performed by changing the spark gap according to experiments, and simulated ignition energies perfectly agree with experimental measurements for hydrogen concentration 10% by vol. in air and $L_{gap} = 2.0$ mm, and concentration 14% for $L_{gap} = 1.0$ mm [8]. Experimental data for rich mixtures are predicted conservatively by simulations. The slight difference may be associated to an increase of losses into the circuit resistance and ionisation losses in the experiments, which are not taken into account into modelling. The latter losses would increase for larger released energy [44]. In conclusion, simulations for hydrogen-air mixtures at $T_0 = 288$ K are seen to well reproduce experimental measurements of MIE.

4.3. Flame kernel development

CFD simulations results allow visualising the evolution of the flame kernel. The simulation test with $T_0 = 288$ K, $H_2 = 29\%$ by vol. in air and $L_{gap} = 0.5$ mm is reported here as a representative case. The energy discharge is equivalent to the numerically determined MIE of 15 μJ. Fig. 4a shows the temperature distribution at 1 μs, i.e. at the end of the energy deposition. The recorded maximum temperature is 2300 K. Fig. 4b shows the associated OH mole fraction distribution, which records a maximum in of about $5 \bullet 10^{-6}$.

Distributions of temperature and OH mole fraction are used to show

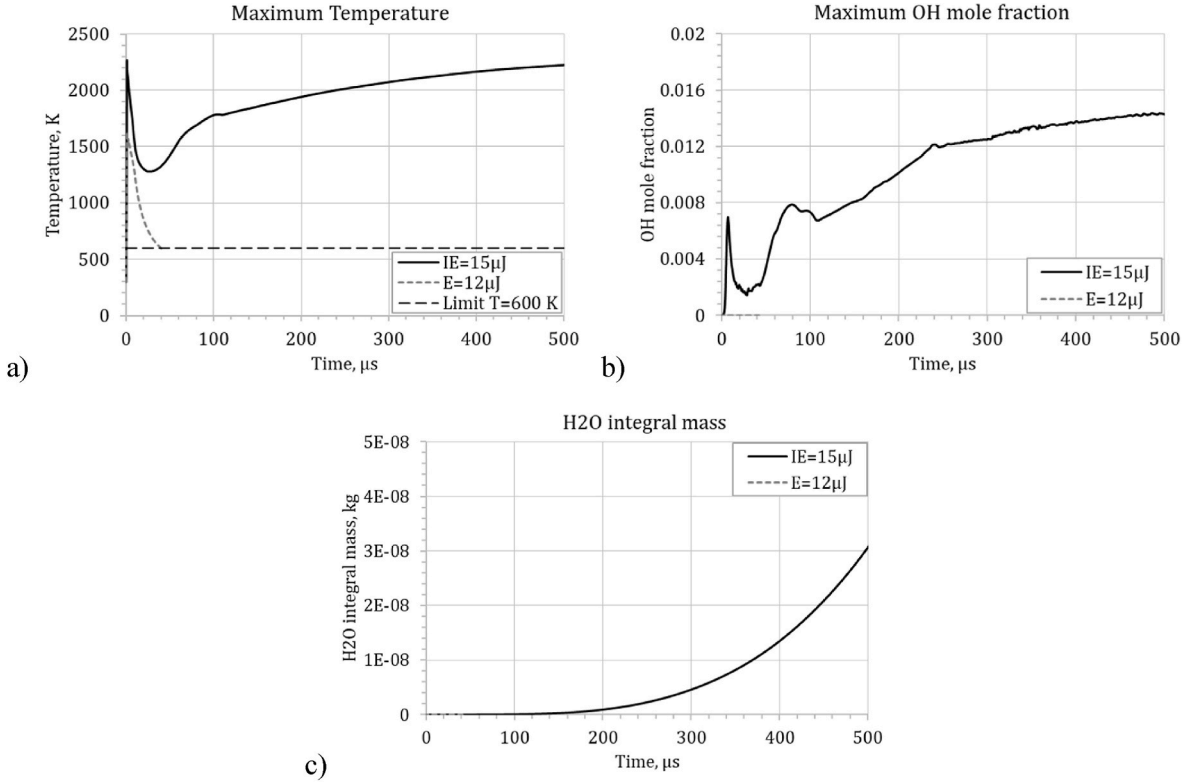

Fig. 2. Assessment of maximum temperature (a), maximum OH mole fraction (b) and H_2O integral mass in the domain (c) for the determination of MIE for $T_0 = 288$ K, 29% hydrogen-air mixture, $R_c = 100$ μm, $R_{el} = 0.1$ mm.

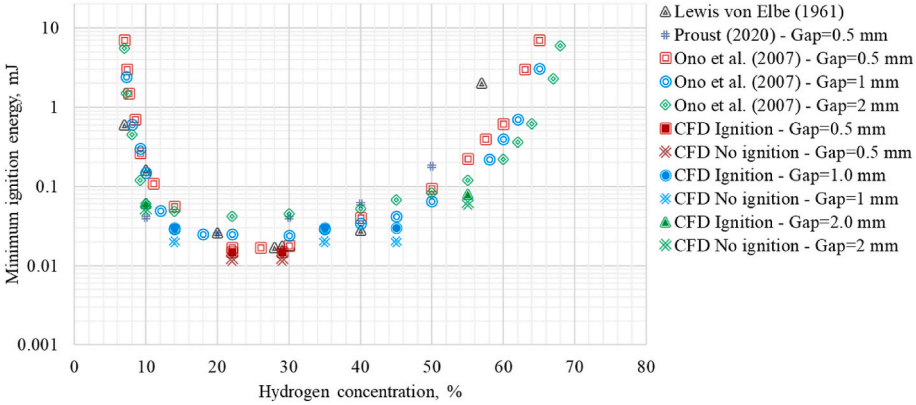

Fig. 3. MIE in hydrogen-air mixture at $T_0 = 288$ K: CFD simulations against experimental data by Refs. [6,8,26].

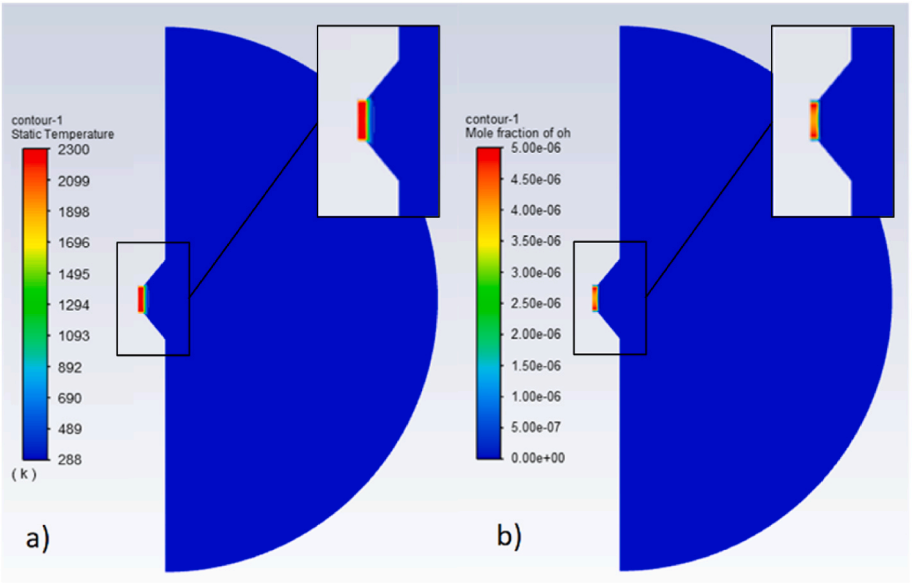

Fig. 4. Distribution of temperature (a) and OH mole fraction (b) on the symmetry plane at 1 μs for $T_0 = 288$ K, 29% hydrogen-air mixture, $L_{gap} = 0.5$ mm, MIE = 15 μJ.

the evolution of the flame kernel in Fig. 5 in the time interval from 45 μs to 500 μs. It can be observed that at 45 μs temperature is higher within the central zone of the spark, because of heat losses to the electrodes. The OH species presence and mole fraction starts to increase at 100 μs, indicating the sustained development of the flame kernel that proceeds to expand spherically. This can also be observed in Fig. 6 for the distributions of temperature and OH species perpendicularly to the axis of the spark channel up to 500 μs. Temperature within and in proximity of the spark channel (up to about 1 mm distance) tends to decrease in time due to heat losses to the electrodes, whereas it increases in correspondence of the flame, which is signalled by the presence of OH species. As expected, the temperature profile at the flame front follows that of OH species. The temperature distribution shows that the flame front tends to stabilise at a temperature of approximately 2200 K (see Fig. 6), whereas the adiabatic flame temperature is equal to 2388 K. The lower temperature in simulations is caused by the radiative and conductive losses to the electrodes. The OH mole fraction distribution along the same direction (see Fig. 6) indicates flame front location in time. The flame propagation velocity is estimated to be about 12 m/s in numerical simulations, whereas analytical estimation using Cantera v.2.4.0 software [45] with GRI 3.0 chemical mechanisms results in about 14.3 m/s. The reason for this discrepancy is thought to be due to three-dimensionality of the flame propagating outwards the spark channel in numerical simulations, which includes flame stretch, and losses to the electrodes, whereas theoretical calculations consider a freely propagating adiabatic one-dimensional flame.

4.4. Simulation results for hydrogen-air mixtures at cryogenic temperature

This section presents the results of numerical simulations to estimate numerically the MIE in cryogenic hydrogen-air mixtures following the same procedure as for ambient temperature mixtures. The numerical tests were conducted on H_2-air mixtures with concentration 20–60% H_2 by vol. (see Table 2). All simulations and experiments for the mixtures at cryogenic temperature are performed for $L_{gap} = 0.5$ mm. Fig. 7 shows the comparison of numerically determined MIE against experimentally measured [26] at the initial mixture temperature 173 K. The experiments were performed within the PRESLHY project and are also reported in Ref. [25]. The numerical MIE is seen to increase from 15 μJ to 30 μJ when the initial temperature decreases from $T_0 = 288$ K to $T_0 = 173$ K, confirming the trend observed in experiments. A deposition of energy equal to 23 μJ failed to ignite the mixture for simulations at $T_0 = 173$ K. The simulated MIE is more conservative compared to the experimental measurements for hydrogen concentrations in the range 20–30% vol. in air, which recorded MIE = 46 μJ for $H_2 = 30\%$ vol. in air.

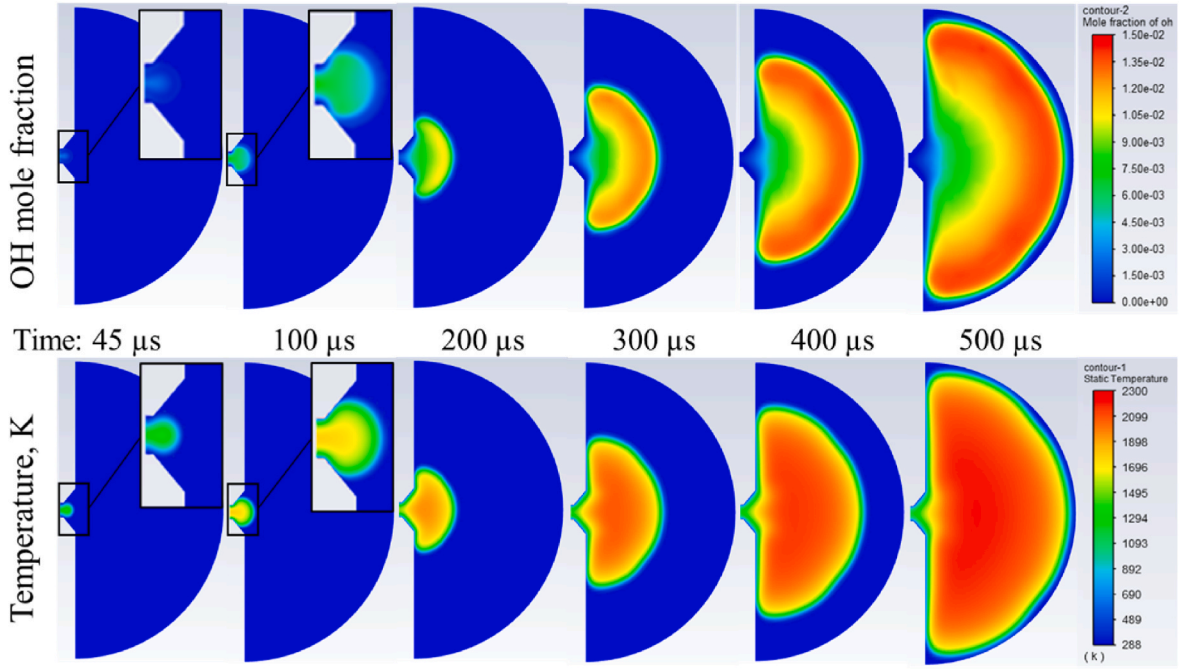

Fig. 5. Flame kernel development for $T_0 = 288$ K, 29% hydrogen-air mixture, $L_{gap} = 0.5$ mm, MIE = 15 µJ.

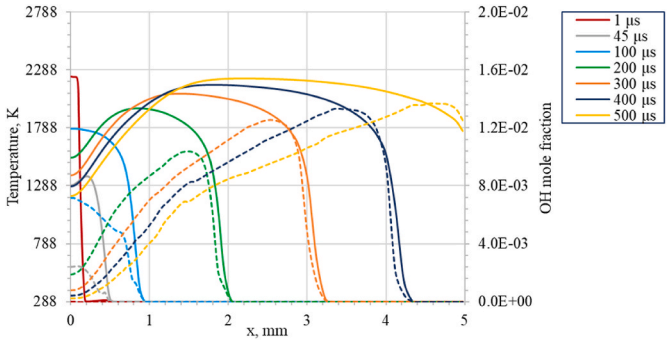

Fig. 6. Distribution of temperature (solid lines) and OH mole fraction (dashed lines) perpendicularly to the spark channel axis for $T_0 = 288$ K, 29% hydrogen-air mixture, $L_{gap} = 0.5$ mm, MIE = 15 µJ.

For higher hydrogen concentration of H_2 = 40% vol. numerical simulations result in IE equal to 30 µJ as per a stoichiometric mixture, which is lower than the experimental measurement. Nevertheless, the lower number of tests conducted for $H_2 = 40\%$ vol. may not be sufficient to estimate accurately the MIE and assess the predictive capability of the numerical model. It should be remarked as well, that simulations do not take into account the losses into the circuit resistance and ionisation losses that may occur in the experiments and would increase for larger released energy [44].

A set of numerical tests were conducted on mixtures of hydrogen with air at initial cryogenic $T_0 = 123$ K. The numerical MIE is found to be equal to 40 µJ for the mixture 20–30% H_2 vol. in air, whereas an energy of 30 µJ is not sufficient to ignite the mixture. Experimental measurements of MIE for $H_2 = 20$–30% vol. in air are available only down to 158 K, recording MIE = 60 µJ [25]. Prediction of MIE by the validated theoretical tool [25] provides MIE = 104 µJ for $H_2 = 20\%$ vol. in air at $T_0 = 123$ K. Discrepancy between numerical simulations and theoretical calculations or experimental measurements could be associated with the numerical assumptions on the spark channel radius and discharge duration, which could differ for very low temperature T_0 = 123 K.

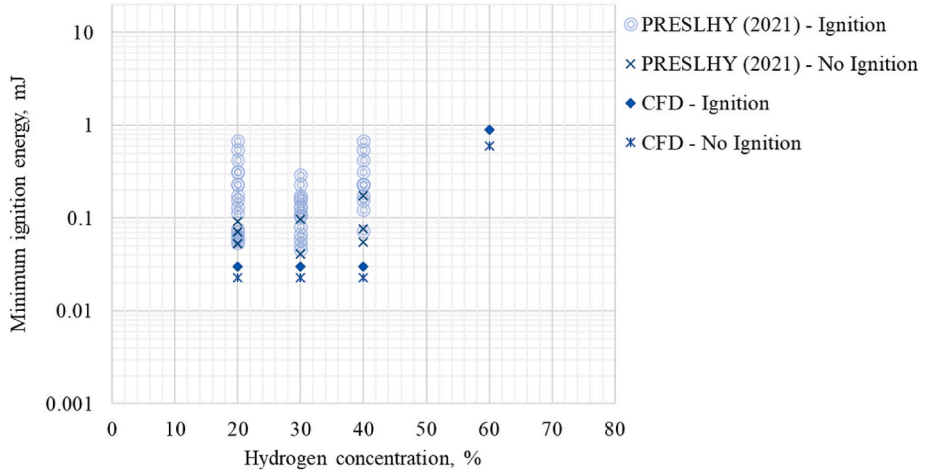

Fig. 7. MIE in hydrogen-air mixture at $T_0 = 173$ K: CFD simulations against PRESLHY experiments (2021) [25].

Further experiments are required to clarify these aspects and consolidate the basis for more accurate assumptions of numerical studies at such low temperatures. It should be remarked, nevertheless, that the complexity of the problem under investigation and the high sensitivity of measurements to the experimental device parameters could lead up to one order of magnitude of deviation in MIE as noted by comparison with experimental data [6,8].

Fig. 8 shows the flame kernel growth in the time interval 50–660 μs through the temperature and OH concentration distributions for the numerical test with $T_0 = 173$ K, $H_2 = 30\%$ vol. in air, $L_{gap} = 0.5$ mm, *MIE* = 30 μJ. The spherically expanding flame front presents some disturbances, whereas these were not noticeable for the ignition test at $T_0 =$ 288 K shown in Fig. 5. The disturbances are believed to be associated with combustion instabilities enhanced by mixture's low temperature. These observations are deemed to support the considerations withdrawn by the theoretical modelling in Ref. [25] hypothesizing the enhancement of flame stretch and preferential diffusion effects and instabilities for hydrogen-air mixtures at lower temperature. The boundaries of the domain are reached by the flame in 660 μs, whereas a minor time was required by the flame in the ambient temperature numerical tests (500 μs).

Fig. 9 shows the temperature and OH concentration distributions perpendicularly to the spark channel axis. Temperature of approximately 4000 K (not visible in Fig. 9) is achieved during the first 1 μs corresponding to the spark duration. Once the energy discharge is stopped, the heat losses and gas expansion lead to a quick decrease in temperature, until flame propagation starts, and temperature increases again. It can be observed that the flame front is established at a temperature of approximately 2100 K. As observed for mixtures at $T_0 = 288$ K, this value is lower than the adiabatic flame temperature (2323 K). At 500 μs the simulated flame propagation velocity is about 9.9 m/s, but since this is seen to not be yet stabilised and to have an increasing trend, it is considered that a larger domain should be used for accurate estimation of the flame propagation velocity.

In conclusion, the developed CFD model is widely validated through comparison with experimental MIE curve for H_2-air mixture at ambient temperature, and is proved to be a suitable and reliable predictive tool for the use of stakeholders in hydrogen safety complementarily to the simpler theoretical tool developed in Ref. [25]. The application of the developed CFD approach is also extended to cryogenic mixtures of hydrogen with air, as capable to capture the dependency of MIE on the mixture temperature and provide conservative MIE assessment. Nevertheless, further experimental research should be performed for lower mixture temperature (below 173 K) to clarify the behaviour of a flame development during ignition.

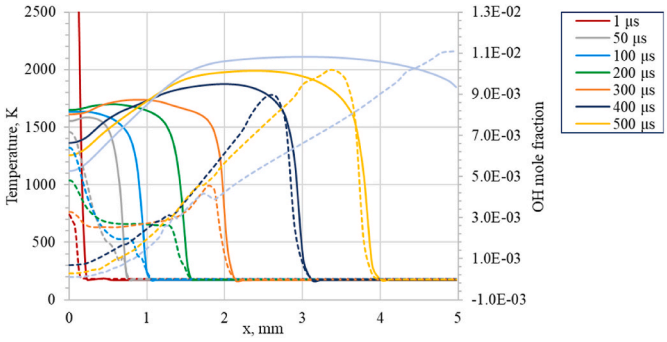

Fig. 9. Distribution of temperature (solid lines) and OH mole fraction (dashed lines) perpendicularly to the spark channel axis for $T_0 = 173$ K, $H_2 = 30\%$ by vol. in air, $L_{gap} = 0.5$ mm, MIE = 30 μJ.

5. Conclusions

The research *originality* resides in the provision of a CFD three-dimensional approach to model spark ignition phenomenon for mixtures at arbitrary initial conditions of hydrogen concentration in air and temperature, including cryogenic mixtures, and determine the resulting MIE. The novel CFD approach takes into account the effect of radiative losses and conductive heat losses to the electrodes.

The research *significance* is established by the provision of a validated CFD approach for the use of stakeholders in safety engineering to estimate numerically the ignition potential of mixtures of hydrogen with air at arbitrary concentration and temperature for a given energy deposition and "electrodes" configuration. The CFD model is further intended to complement the theoretical modelling tool for determination of MIE developed by the authors [25].

A wide set of experiments available in literature for mixtures at initial ambient temperature was used for the validation of the novel CFD approach, establishing the research *rigour*. The validity of the model was expanded to mixtures of hydrogen with air at 173 K through comparison against the INERIS cryogenic experimental tests performed within the

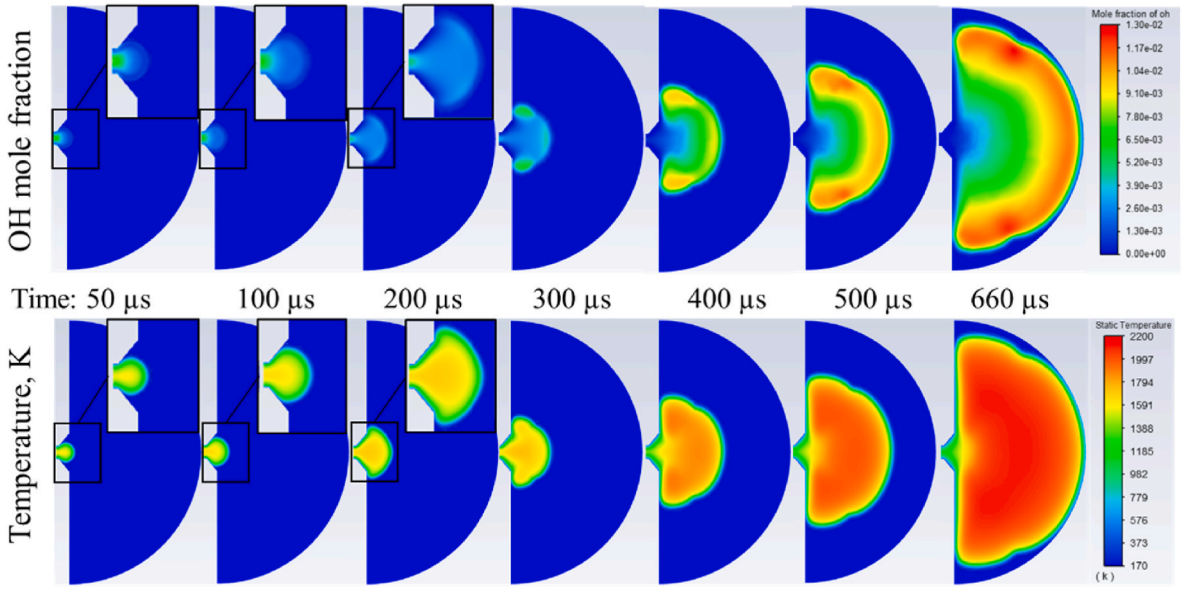

Fig. 8. Flame kernel development for $T_0 = 173$ K, 30% hydrogen-air mixture, $L_{gap} = 0.5$ mm, MIE = 30 μJ.

project PRESLHY [25,26]. The CFD model reproduced accurately the MIE experimental measurements for both ambient and cryogenic initial temperature of the mixture. Results of numerical simulations showed a decrease of MIE with the increase of initial temperature, in line with theoretical and experimental conclusions in Ref. [25]. Therefore, it is deemed that current safety measures established for ambient temperature mixtures can conservatively be implemented for cryogenic applications. To further establish the rigour of the research, the study included a parametric assessment to examine the impact of relevant numerical and experimental details on modelling results. It is deemed that CFD modelling should always include conductive heat losses to the electrodes, as they were observed to affect the numerical outcomes. Inclusion of radiation modelling was found to impact significantly the temperature achieved for the high energy deposits and this is considered to potentially affect the numerically determined MIE and the flame kernel development. Furthermore, experimental evidence demonstrated the MIE dependence on the electrodes' gap distance. It is fundamental for numerical simulations to consider a configuration representing as much as possible the experimental design to accurately reproduce measured MIE.

CRediT authorship contribution statement

Donatella Cirrone: Writing – original draft, Visualization, Validation, Software, Resources, Methodology, Investigation, Formal analysis, Data curation, Conceptualization. **Dmitriy Makarov:** Writing – review & editing, Validation, Supervision, Resources, Methodology, Investigation, Conceptualization. **Christophe Proust:** Writing – review & editing, Validation, Resources, Investigation, Formal analysis, Data curation. **Vladimir Molkov:** Writing – review & editing, Validation, Supervision, Project administration, Methodology, Investigation, Funding acquisition, Formal analysis, Conceptualization.

Declaration of competing interest

The authors declare that they have no known competing financial interests or personal relationships that could have appeared to influence the work reported in this paper.

Acknowledgments

The authors would like to express their gratitude to Professor Ryo Ono for sharing his expertise and information regarding the performed experiments. This research has received funding from the Fuel Cells and Hydrogen 2 Joint Undertaking (now Clean Hydrogen Partnership) under the European Union's Horizon 2020 research and innovation programme under grant agreement No. 779613 (PRESLHY). The authors would like to acknowledge EPSRC for funding the project Kelvin-2 "Tier 2 High-Performance Computing Services", EP/T022175/1.

References

[1] ASTM. ASTM E582-21. Standard test method for minimum ignition energy and quenching distance in gaseous mixtures. https://doi.org/10.1520/E0582-21; 2021.
[2] Kumamoto A, Iseki H, Ono R, Oda T. Measurement of minimum ignition energy in hydrogen-oxygen-nitrogen premixed gas by spark discharge. J Phys Conf Ser 2011; 301. https://doi.org/10.1088/1742-6596/301/1/012039.
[3] Pratt TH. Electrostatic ignitions of fires and explosions. New York, NY: Center for Chemical Process Safety of the American Institute of Chemical Engineers; 2000.
[4] Terao K. Irreversible phenomena. Ignitions, combustion and detonation waves. Springer; 2007.
[5] Calcote HF, Gregory CA, Barnett CM, Gilmer RB. Spark ignition. Effect of molecular structure. Ind Eng Chem 1952;44:2656–62. https://doi.org/10.1021/ie50515a048.
[6] Lewis B, Elbe G von. Combustion, flames and explosions of gases, 36. New York: Academic Press; 1961. https://doi.org/10.1524/zpch.1963.36.3_4.136.
[7] ISO/TR 15916:2015. Basic considerations for the safety of hydrogen systems. 2015.
[8] Ono R, Nifuku M, Fujiwara S, Horiguchi S, Oda T. Minimum ignition energy of hydrogen-air mixture: effects of humidity and spark duration. J Electrost 2007;65: 87–93. https://doi.org/10.1016/j.elstat.2006.07.004.
[9] Kuchta JM. Investigation of fire and explosion accidents in the chemical, mining, and fuel-related industries. A manual. US Bur Mines Bull; 1985. 680.
[10] Babrauskas V. Ignition handbook. Issaquah WA, USA: society of fire protection engineers. Fire Science Publishers; 2003.
[11] Rose HE, Priede T. Ignition phenomena in hydrogen-air mixtures. Symp. Combust. 1958;7:436–45.
[12] Witcofski RD, Chirivella JE. Experimental and analytical analyses of the mechanisms governing the dispersion of flammable clouds formed by liquid hydrogen spills. Int J Hydrogen Energy 1984;9:425–35.
[13] Hall JE, Hooker P, Willoughby D. Ignited releases of liquid hydrogen: safety considerations of thermal and overpressure effects. Int J Hydrogen Energy 2014; 39:20547–53. https://doi.org/10.1016/j.ijhydene.2014.05.141.
[14] Maly RR, Herweg R. Spark ignition and combustion in four-stroke gasoline engines. Flow combust. Reciprocating engines. Berlin Heidelberg: Springer; 2009. https://doi.org/10.1007/978-3-540-68901-0.
[15] Bane SPM. Spark ignition: experimental and numerical investigation with application to aviation safety. Dissertation (Ph.D.). California Institute of Technology; 2010. https://doi.org/10.7907/W1NB-5W06.
[16] Liberman MA. Introduction to physics and chemistry of combustion. Explosion, flame, detonation. Berlin: Springer; 2008. https://doi.org/10.1007/978-3-540-78759-4.
[17] Frendi A, Sibulkin M. Dependence of minimum ignition energy on ignition parameters. Combust Sci Technol 1990;73:395–413.
[18] Thiele M, Warnatz J, Dreizler A, Lindenmaier S, Schießl R, Maas U, et al. Spark ignited hydrogen/air mixtures: two dimensional detailed modeling and laser based diagnostics. Combust Flame 2002;128:74–87. https://doi.org/10.1016/S0010-2180(01)00333-9.
[19] Yuasa T, Kadota S, Tsue M, Kono M, Nomura H, Ujiie Y. Effects of energy deposition schedule on minimum ignition energy in spark ignition of methane/air mixtures. Proc Combust Inst 2002;29:743–50. https://doi.org/10.1016/S1540-7489(02)80095-5.
[20] Han J, Yamashita H, Yamamoto K. Numerical study on spark ignition characteristics of a methane-air mixture using detailed chemical kinetics (effect of electrode temperature and energy channel length on flame propagation and relationship between minimum ignition energy and equivalence ra. J Therm Sci Technol 2009;4:305–13. https://doi.org/10.1299/jtst.4.305.
[21] Han J, Yamashita H, Hayashi N. Numerical study on the spark ignition characteristics of a methane-air mixture using detailed chemical kinetics. Effect of equivalence ratio, electrode gap distance, and electrode radius on MIE, quenching distance, and ignition delay. Combust Flame 2010;157:1414–21. https://doi.org/10.1016/j.combustflame.2010.02.021.
[22] Han J, Yamashita H, Hayashi N. Numerical study on the spark ignition characteristics of hydrogen-air mixture using detailed chemical kinetics. Int J Hydrogen Energy 2011;36:9286–97. https://doi.org/10.1016/j.ijhydene.2011.04.190.
[23] Fernández-Tarrazo E, Gómez-Miguel R, Sánchez-Sanz M. Minimum ignition energy of hydrogen–ammonia blends in air. Fuel 2023;337:127128. https://doi.org/10.1016/j.fuel.2022.127128.
[24] Office of Energy Efficiency & Renewable. Physical hydrogen storage. https://www.energy.gov/eere/fuelcells/physical-hydrogen-storage; 2022.
[25] Cirrone D, Makarov D, Proust C, Molkov V. Minimum ignition energy of hydrogen-air mixtures at ambient and cryogenic temperatures. Int J Hydrogen Energy 2023; 48:16530–44. https://doi.org/10.1016/j.ijhydene.2023.01.115.
[26] Proust C. A new technique to produce well controlled electrical sparks. Application to MIE measurements. In: 13th int. Symp. Hazards, prev. Mitig. Ind. Explos; 2020. Braunschweig, Germany.
[27] Ono R. Private communication. 2019.
[28] Proust C, Jamois D. Some fundamental combustion properties of "cryogenic" premixed hydrogen air flames. In: ID32. Int. Conf. Hydrog. Saf.; 2021. p. 1–12. Edinburgh, Scotland, UK.
[29] Peters N, Rogg B. Reduced kinetic mechanisms for applications in combustion systems. 1993. Berlin. Berlin.
[30] Murthy JY, Mathur SR. A finite volume method for radiative heat transfer using unstructured meshes. 36th AIAA Aerosp Sci Meet Exhib 1998;M. https://doi.org/10.2514/6.1998-860.
[31] Cirrone D, Makarov D, Lach AW, Gaathaug AV, Molkov V. The pressure peaking phenomenon for ignited under-expanded hydrogen jets in the storage enclosure: experiments and simulations for release rates of up to 11.5 g/s. Energies 2022;15: 1–20.
[32] Cirrone D, Makarov D, Molkov V. Thermal radiation from cryogenic hydrogen jet fires. Int J Hydrogen Energy 2019;44:8874–85. https://doi.org/10.1016/j.ijhydene.2018.08.107.
[33] Cirrone D, Makarov D, Kuznetsov M, Friedrich A, Molkov V. Effect of heat transfer through the release pipe on simulations of cryogenic hydrogen jet fires and hazard distances. Int J Hydrogen Energy 2022;47:21596–611. https://doi.org/10.1016/j.ijhydene.2022.04.276.
[34] Bane SPM, Ziegler JL, Boettcher PA, Coronel SA, Shepherd JE. Experimental investigation of spark ignition energy in kerosene, hexane, and hydrogen. J Loss Prev Process Ind 2013;26:290–4. https://doi.org/10.1016/j.jlp.2011.03.007.
[35] Benmouffok M, Freton P, Gonzalez JJ. Theoretical plasma characterization during current pulse. IJRRAS 2018;34.
[36] Quantum engineering and design. Tungsten 2023. http://qedfusion.org/LIB/PROPS/PANOS/w.html.
[37] The Engineering Toolbox. Surface emissivity coefficients. https://www.engineeringtoolbox.com/emissivity-coefficients-d_447.html; 2023.
[38] Fluent A. User's guide. 2016.

[39] Molkov VV, Cirrone DMC, Shentsov VV, Dery W, Kim W, Makarov DV. Dynamics of blast wave and fireball after hydrogen tank rupture in a fire in the open atmosphere. Int J Hydrogen Energy 2021;46:4644–65. https://doi.org/10.1016/j.ijhydene.2020.10.211.
[40] Hubbard C, Tien GL. Infrared mean absorption coefficients of luminous flames and smoke. J Heat Tran 1978;100:235–9.
[41] Yang Y. Plasma discharge in water and its application for industrial cooling water treatment. 2011.
[42] Kim HJ, Hong SW, Kim HD. Quenching distance measurement for the control of hydrogen explosion. Proceedings of the 18th Int. Colloq. Dyn. Explos. React. Syst. Paper 2001;191.
[43] Cirrone D, Makarov D, Molkov V. Spontaneous ignition of cryo-compressed hydrogen in a T-shaped channel system. Hydro 2022;3:348–60. https://doi.org/10.3390/hydrogen3030021.
[44] Jarosinski J, Veyssiere B. Combustion phenomena: selected mechanisms of flame formation, propagation and extinction. 2009.
[45] Goodwin DG, Moffat HK, Schoegl I, Speth RL, Weber BW. Cantera: an object-oriented software toolkit for chemical kinetics, thermodynamics, and transport processes. 2021. https://doi.org/10.5281/zenodo.6387882., V 2.4.0.